Letter

Magnetic structure of RuO_2 in view of altermagnetism

S. W. Lovesey,[1,2,3] D. D. Khalyavin,[1] and G. van der Laan[2]
[1]*ISIS Facility, STFC, Didcot, Oxfordshire OX11 0QX, United Kingdom*
[2]*Diamond Light Source, Harwell Science and Innovation Campus, Didcot, Oxfordshire OX11 0DE, United Kingdom*
[3]*Department of Physics, Oxford University, Oxford OX1 3PU, United Kingdom*

(Received 20 June 2023; revised 30 July 2023; accepted 25 August 2023; published 5 September 2023)

The magnetic structure of RuO_2 and the Ru atomic configuration are unknown. A magnetic structure is inferred by confronting measured and calculated Bragg diffraction patterns and adjusting the latter to achieve satisfactory agreement. An accepted pattern, a magnetic symmetry, includes symmetry of sites occupied by the magnetic ions. As a realistic starting point, we provide diffraction patterns for a magnetic symmetry of RuO_2, a descendent of the tetragonal parent structure, which accommodates a departure of Ru axial dipoles from the crystal c axis. A chiral signal and piezomagnetic effect are permitted, and a linear magnetoelectric effect forbidden. Features of the neutron diffraction pattern test the nonrelativistic requirement of altermagnetism, and we scrutinize published room-temperature data. Specifically, one Bragg point is consistent with Ru orbital angular momentum and magnetic quadrupole both zero, and the latter result is not expected from nonrelativistic altermagnetism. Azimuthal angle scans in resonant x-ray diffraction are sensitive to the Ru site symmetry and the atomic configuration. Acid tests of the studied magnetic symmetry include a chiral signature and null intensity for unrotated photon polarization.

DOI: 10.1103/PhysRevB.108.L121103

I. INTRODUCTION

Ruthenium dioxide is a prominent face of altermagnetism, yet there is no consensus on its magnetic structure or the Ru electronic configuration [1,2]. We frame pertinent questions using a realistic magnetic symmetry, and pose some answers available from diffraction experiments. Altermagnetism is a nonrelativistic theory dedicated to collinear magnetic structures with perfect translation invariance. At face value, the theory is relevant to materials with a negligible spin-orbit coupling in the electronic configuration, and a magnetic structure with a null propagation vector. Spin degrees of freedom are completely decoupled from the lattice in the nonrelativistic space groups of altermagnetism, which include transformations of spins and lattice that are not symmetry elements if one takes into account spin orbit coupling. In consequence, symmetry tools embedded in altermagnetism must be applied consistently to avoid pitfalls from a mix and match theory.

The magnetic axial quadrupole in neutron diffraction is zero if the magnetic atomic state is a single J-state ($\mathbf{J} = \mathbf{S} + \mathbf{L}$ is the total angular momentum), as in the extreme $j_{\rm eff}$ model of iridates with strong spin-orbit coupling [3]. Thus, the observation of a significant magnetic quadrupole in RuO_2 would weigh in favor its description by altermagnetism. Similarly, resonant x-ray diffraction is an excellent probe of local chargelike and magnetic angular anisotropy. According to Neumann's Principle, such anisotropies delineate the local symmetry of resonant ions [4,5]. Thermal transport coefficients calculated for a model of RuO_2 show a striking dependence on the Néel vector derived from neighboring Ru ions in a rutile structure. Specifically, this concerns the temperature dependent anomalous Nernst (thermoelectric), thermal Hall and Hall conductivities [6]. However, Zhou *et al.* [6] find null values for all the transport coefficients for a Néel vector parallel to the crystal c axis, which is demanded by rutile magnetic symmetry ($P4_2'/mnm'$). By adopting a magnetic symmetry for RuO_2 descended from the tetragonal (rutile) crystal structure, the Néel vector is not constrained to the c axis. We give a coherent account of neutron and x-ray diffraction patterns derived from the reduced symmetry to be tested in future experiments.

Centrosymmetric magnetic symmetry $P2_1/c$ chosen for RuO_2 does not break translation symmetry and the propagation vector $\mathbf{k} = (0,\ 0,\ 0)$. It accommodates an antiferromagnetic motif of axial dipole moments in the tetragonal (bc) plane together with a ferromagnetic component along the a axis, as depicted in Fig. 1 (for structure information see the Supplemental Material (SM) [7]). A linear magnetoelectric effect is forbidden, because anti-inversion is absent in the $P2_1/c$ crystal class, and a piezomagnetic effect is allowed. Notably, magnetic symmetry $P2_1/c$ responds to helicity in a beam of photons.

In the following, magnetic properties are referred to orthogonal vectors labeled ($\xi,\ \eta,\ \zeta$) derived from the monoclinic unit cell depicted in Fig. 1. The unique axis η is parallel to the tetragonal a axis. Conventionally, the development of magnetic order leads to a lowering of the symmetry in the sample and the magnetic ordering pattern can be inferred by

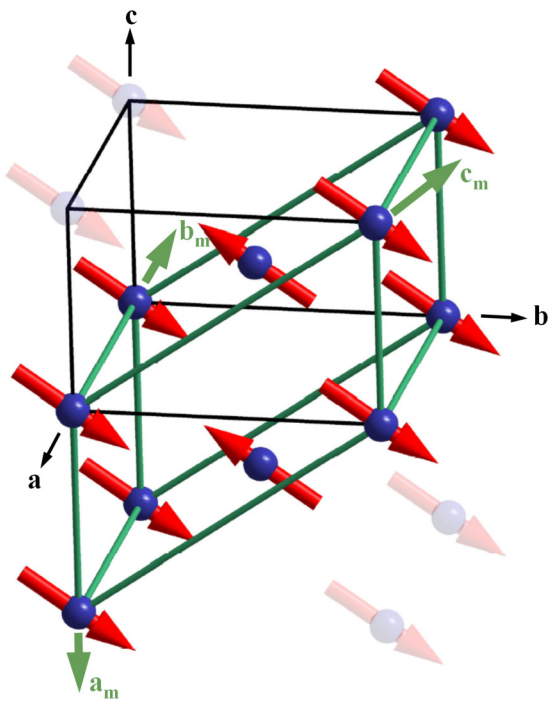

FIG. 1. Tetragonal ($P4_2/mnm$) and monoclinic ($P2_1/c$) unit cells. Vectors are defined in the SM. Magnetic properties are referred to orthogonal vectors (ξ, η, ζ) that match (a^*_m, b_m, c_m) where $\mathbf{a}^*_m$ is a reciprocal lattice vector $\propto (\mathbf{b}_m \times \mathbf{c}_m)$.

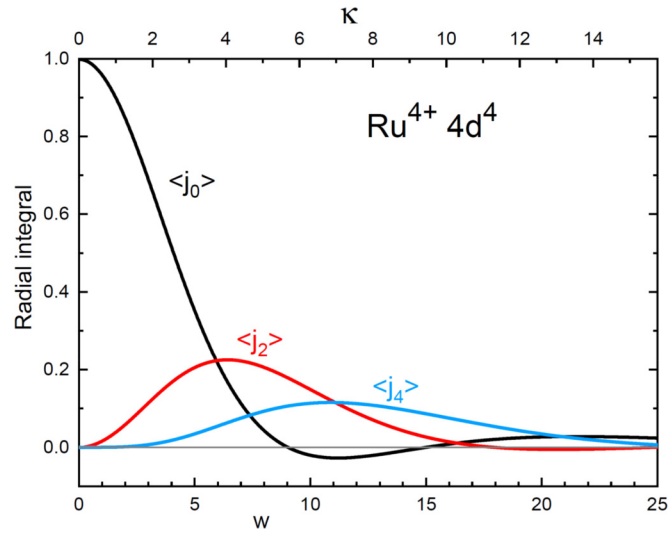

FIG. 2. Radial integrals $\langle j_0\rangle$ (black), $\langle j_2\rangle$ (red), and $\langle j_4\rangle$ (blue) for Ru^{4+} ($4d^4$) calculated using Cowan's code [11,12]. The dimensionless parameter w and the magnitude of the reflection vector κ are related by the Bohr radius, namely, $\kappa = w/3a_o$. Also, $\kappa = 4\pi s$ with $s = \sin(\theta)/\lambda$, Bragg angle θ, and λ the neutron wavelength (cf. Section 6.3.1, Ref. [14]). Reflection vector κ and s in units of $Å^{-1}$.

confronting experimental patterns derived by neutron diffraction with a symmetry analysis in which selected elements of crystal symmetry are assumed to have disappeared. Our results for neutron and x-ray diffraction patterns are for Bragg spots forbidden by the core structure, often labeled basis forbidden reflections. By construction, Bragg spots contain only magnetic and aspherical chargelike electronic contributions. Reflection vectors for tetragonal and monoclinic structures are labeled $(H_o,\ K_o,\ L_o)_t$ and $(h,\ k,\ l)_m$, respectively. Basis forbidden reflections possess odd $k + l$, and our subset $l = 0$ is chosen on the grounds of relatively simple analytic diffraction patterns.

II. MAGNETIC QUADRUPOLE

A dependence of the magnetic neutron scattering amplitude on both the magnitude and direction of the reflection vector κ is a most valuable property of the technique. It enables the measurement of the magnetization density, or its spatial Fourier transform more correctly, and the identification of electron back-transfer (covalency) [9,10]. Ruthenium dioxide can be described as a strongly covalent intermediate coupling system, and the Ru atomic configuration is defined by a mixture of J states.

The axial dipole $\langle \mathbf{t}^1\rangle$ contains standard radial integrals $\langle j_0(\kappa)\rangle$ and $\langle j_2(\kappa)\rangle$ depicted in Fig. 2 for the atomic configuration $4d^4$, with $\langle j_0(0)\rangle = 1$ and $\langle j_2(0)\rangle = 0$ [11,12]. They appear in both atomic and itinerant formulations of magnetic neutron diffraction (cf. Section 7.5 in Ref. [10]). The method used to calculate radial integrals in Fig. 2 is a tried and tested atomic code [11]. Modifications caused by electron back-transfer have been assessed by Hubbard and Marshall [9]. In the case of an itinerant electron system, however, a simulation of the electronic structure is desirable but beyond the scope of the present study.

An approximation to $\langle \mathbf{t}^1\rangle$,

$$\langle \mathbf{t}^1\rangle \approx (2/3)\,[\langle j_0(\kappa)\rangle\langle \mathbf{S}\rangle + (1/2)\,(\langle j_0(\kappa)\rangle + \langle j_2(\kappa)\rangle)\,\langle \mathbf{L}\rangle], \tag{1}$$

is often used [10,13]. The numerical coefficient of orbital angular momentum in the ground state $\langle \mathbf{L}\rangle$ is approximate, while $\langle \mathbf{t}^1\rangle = (1/3)\langle 2\mathbf{S} + \mathbf{L}\rangle$ for $\kappa \to 0$ is an exact result. Equation (1) implies $\langle \mathbf{t}^1\rangle = 0$ for d^4, because the atomic configuration is a singlet $J = 0$. One finds a magnetic moment $\langle \mu_\zeta\rangle = \langle (2\mathbf{S} + \mathbf{L})_\zeta\rangle = -\langle \mathbf{L}_\zeta\rangle = \chi(1)_0\sqrt{2}$, $\langle t^1_\zeta\rangle = (1/3)\langle \mu_\zeta\rangle[\langle j_0(\kappa)\rangle - (3/4)\langle j_2(\kappa)\rangle]$ using $J = 0$ and $J' = 1$, and a purely real mixing parameter $\chi(1)_0$ [13]. Remaining components of the dipole are enabled by $J' = 1$, $M' = +1$, and they are $\langle t^1_\xi\rangle = \sqrt{2}\{\chi(1)'_1/\chi(1)_0\}\langle t^1_\zeta\rangle$ and $\langle t^1_\eta\rangle = \sqrt{2}\{\chi(1)''_1/\chi(1)_0\}\langle t^1_\zeta\rangle$, where a single prime and double prime denote the real and imaginary parts of the mixing parameter χ_1, respectively. All foregoing results for $\langle \mathbf{t}^1\rangle$ are exact, and the form factor $[\langle j_0(\kappa)\rangle - (3/4)\langle j_2(\kappa)\rangle]$ is common to components of the Néel vector.

Next in line is a quadrupole and another valuable property, namely, multipoles of even rank are identically zero in a J manifold. The j_{eff} model of an iridate is a relevant example [3,13]. The total angular momentum of an Ir ion is $J = 5/2$ and the corresponding quadrupole $\langle \mathbf{t}^2\rangle = 0$. However, a realistic model of Sr_2IrO_4, say, allows for a distortion of the environment along the c axis and $J = 3/2$ contaminates the $J = 5/2$ state and $\langle \mathbf{t}^2\rangle$ is nonzero. Specifically, the quadrupole depends on the electronic position operator $\mathbf{n}$. The equivalent operator $[(\mathbf{S} \times \mathbf{n})\ \mathbf{n}]$ for $\mathbf{t}^2$ shows it is a measure the correlation between the spin anapole $(\mathbf{S} \times \mathbf{n})$ and orbital degrees of freedom [3,13]. A quadrupole has five components

labeled by projections $Q = 0,\ \pm1,\ \pm2$. Ruthenium site symmetry does not restrict Q, for there is no spatial awareness other than a centre of inversion symmetry that forbids parity-odd Dirac multipoles [13]. Diagonal $Q = 0$ components of axial multipoles of rank K in neutron diffraction are identically zero for even K and d^4. Moreover, the rank K obeys the selection rule $K = J'$ in d^4 [13]. The atomic configuration of Ru^{4+} includes $J = 0$ and $J' = 2$. We find the exact results $\langle t^2_{\pm1}\rangle = \{i\chi(2)_1/4\}\ \sqrt{(5/7)}\langle j_2(\kappa)\rangle$, $\langle t^2_{\pm2}\rangle = \{\chi(2)_2/\chi(2)_1\}\ \langle t^2_{\mp1}\rangle$, where $\chi(2)_1$ and $\chi(2)_2$ are the mixing parameter for $M' = +1$ and $M' = +2$, respectively, in the state $J' = 2$. In subsequent work, we restrict attention to dipoles and quadrupoles, setting aside octupoles and hexadecapoles allowed in d^4 amplitudes. The octupole form factor using $J = 0$ and $J' = 3$ is $[\langle j_2(\kappa)\rangle + (3/8)\langle j_4(\kappa)\rangle]$, and a hexadecapole is proportional to $\langle j_4(\kappa)\rangle$ [13].

The amplitude of magnetic neutron diffraction $\langle \mathbf{Q}_\perp\rangle = [\langle \mathbf{Q}\rangle - \mathbf{e}(\mathbf{e}\bullet\langle \mathbf{Q}\rangle)]$ yields an intensity $|\langle \mathbf{Q}_\perp\rangle|^2 = |\langle \mathbf{Q}\rangle|^2 - |(\mathbf{e}\bullet\langle \mathbf{Q}\rangle)|^2$, where the unit vector $\mathbf{e} = \boldsymbol{\kappa}/\kappa$ [9,10]. Factors required to relate $|\langle \mathbf{Q}_\perp\rangle|^2$ to the measured intensity of a Bragg spot can be found in Ref. [14]. We use a shorthand $c = \cos(\beta) = \cos(124.662^\circ) = -0.57$ and $s = \sin(\beta) = +0.82$, where β is the obtuse angle of the monoclinic cell in Fig. 1. Basis forbidden reflections include $\boldsymbol{\kappa} = (0,\ 0,\ L_o)_t$ with odd L_o. In this case $\langle Q_\eta\rangle \approx 0$ and,

$$\langle Q_{\perp\xi}\rangle \approx c\{[c\langle t^1_\xi\rangle - s\langle t^1_\zeta\rangle] + f\},$$
$$\langle Q_{\perp\zeta}\rangle \approx -s\{[c\langle t^1_\xi\rangle - s\langle t^1_\zeta\rangle] + f\}. \qquad (2)$$

Here, $f = (2/\sqrt{3})[c\ \langle t^2_{+1}\rangle'' - s\langle t^2_{+2}\rangle'']$, with $\langle t^2_{+1}\rangle'' \propto (\eta\zeta)$ and $\langle t^2_{+2}\rangle'' \propto (\xi\eta)$ for quadrupole spatial awareness obtained from a spherical harmonic of rank 2. Amplitudes in Eq. (2) contain axial dipoles that form the Néel vector, and the same is true of all basis-forbidden amplitudes, i.e., the ferromagnetic component using $\langle t^1_\eta\rangle$ is not observed at basis-forbidden reflections with monoclinic Miller indices $k + l = 2m + 1$.

Berlijn *et al.* [15] did not find measurable intensities for reflection vectors $(0,\ 0,\ 1)_t$ and $(0,\ 0,\ 3)_t$ and conclude that dipole moments are parallel to the c axis of rutile ($P4_2'/mnm'$). Setting $f = 0$ in Eq. (2), and $c\ \langle t^1_\xi\rangle = s\langle t^1_\zeta\rangle$ for null amplitudes places $\langle \mathbf{t}^1\rangle$ parallel to the crystal c axis. Inclusion of quadruples changes the result for the orientation of the axial dipole. Returning to Eq. (2), a null intensity implies $\{[c\ \langle t^1_\xi\rangle - s\ \langle t^1_\zeta\rangle] + f\} = 0$, and in the corrected theory of diffraction $\langle \mathbf{t}^1\rangle$ subtends an angle $\approx -s(f/\langle t^1_\zeta\rangle)$ to the c axis. Evidently, a significant factor in the magnitude of the deflection from the c axis is the ratio $\langle j_2(\kappa)\rangle/\langle j_0(\kappa)\rangle$ for which we find the value 0.193 at $(0,\ 0,\ 1)_t$. With regard to $(0,\ 0,\ 3)_t$, we see from Fig. 2 that $\langle j_0(\kappa)\rangle \approx 0$, to a good approximation, while $\langle j_2(\kappa)\rangle = 0.16$. Null $(0,\ 0,\ 3)_t$ intensity infers that the projection of $\langle \mathbf{t}^1\rangle$ on the c axis is $\{(1 - s\ p)/\sqrt{[1 + p\ (p - 2s)]}\}$ with $p = (3f/\langle j_2(\kappa)\rangle\ \langle L_\zeta\rangle)$ and nonzero orbital angular momentum. An equally viable interpretation of a null $(0,\ 0,\ 3)_t$ intensity, and $\langle j_2(\kappa)\rangle$ different from zero, is $\chi(2)_r = 0$ in the state $J' = 2$, and zero orbital angular momentum from $\chi(1)_r = 0$.

Moving on, Berlijn *et al.* observed magnetic intensity at reflections $(1,\ 0,\ 0)_t$ and $(3,\ 0,\ 0)_t$ [15]. For $\boldsymbol{\kappa} = (0,\ k,\ 0)_m \equiv (-k,\ 0,\ 0)_t$ with $k = 2m + 1$ we obtain relatively simple amplitudes,

$$\langle Q_{\perp\xi}\rangle \approx \langle t^1_\xi\rangle - (2/\sqrt{3})\langle t^2_{+1}\rangle'',\ \langle Q_{\perp\eta}\rangle \approx 0,$$
$$\langle Q_{\perp\zeta}\rangle \approx \langle t^1_\zeta\rangle - (2/\sqrt{3})\langle t^2_{+2}\rangle'', \qquad (3)$$

since $(\mathbf{e}\bullet\langle \mathbf{Q}\rangle) = 0$. Amplitudes Eq. (3) await a test. Individual components of $\langle \mathbf{Q}_\perp\rangle$ can be selected for observation in the spin-flip signal (SF) $= \{|\langle \mathbf{Q}_\perp\rangle|^2 - |\mathbf{P}\bullet\langle \mathbf{Q}_\perp\rangle|^2\}$, where neutron polarization $\mathbf{P}$ is assumed to be perfect. And, for future experiments using $\boldsymbol{\kappa} = (0,\ 0,\ l)_m \equiv (0,\ l,\ 0)_t$ with $l = 2m + 1$,

$$\langle Q_\xi\rangle \approx \langle t^1_\xi\rangle + (2/\sqrt{3})\,s\,[s\langle t^2_{+1}\rangle'' + c\langle t^2_{+2}\rangle''],\ \langle Q_\eta\rangle \approx 0,$$
$$\langle Q_\zeta\rangle \approx \langle t^1_\zeta\rangle + (2/\sqrt{3})\,c\,[s\langle t^2_{+1}\rangle'' + c\langle t^2_{+2}\rangle''], \qquad (4)$$

with $(\mathbf{e}\bullet\langle \mathbf{Q}\rangle) = s\ \langle t^1_\zeta\rangle - c\ \langle t^1_\xi\rangle$. Quadrupoles in Eqs. (2) and (4) occur in different combinations.

III. CHIRAL SIGNATURE

The magnetic symmetry considered for RuO_2 permits coupling with circular polarization in the primary beam of x-rays [16]. The coupling equates to a chiral signature for the symmetry and it demands a centrosymmetric crystal, magnetic order that does not break translation symmetry, and absence of anti-inversion ($\bar{1}'$) in the magnetic crystal class. Note that the latter demand rules out a linear magnetoelectric effect as a material property. A symmetry analysis of a parity-even absorption event shows that the corresponding chiral signature is caused by an interference between chargelike (time-even) and magnetic (time-odd) multipoles. At the level of accuracy to which we work, the signal is an interference between dipoles and chargelike quadrupoles, which create Templeton-Templeton scattering. In practice, the signature is captured in a difference between Bragg spot intensities measured with opposite handed primary x-rays.

Our results for resonant x-ray diffraction amplitudes exploit universal expressions [17]. In line with standard practice, primary photon polarizations labeled σ and π are perpendicular and parallel to the plane of scattering, respectively, and secondary polarization carry a prime [18–21]. Regarding diffraction amplitudes, $(\pi'\sigma)$ and $(\sigma'\sigma)$ apply to primary σ polarization rotated to the π channel and returned to the σ channel, respectively. In the diffraction setting crystals are rotated around the reflection vector by an angle ψ (an azimuthal angle scan). In contrast to neutron diffraction, the fixed x-ray energy severely limits the number of Bragg spots. Ruthenium L_2 and L_3 absorption edges occur at energies $E \approx 2.97$ keV and $E \approx 2.84$ keV, respectively, and a wavelength $\approx 12.4/E$ Å. Diffraction of x-rays by ruthenium multipoles with enhancement by an electric-dipole–electric-dipole (E1–E1) absorption event is described in terms of multipoles $\langle \mathbf{T}^K\rangle$ with rank $K = 0, 1, 2$. They have a time signature $(-1)^K$, and energy-integrated intensities satisfy sum rules at L_2 and L_3 edges [21,22]. X-ray magnetic circular dichroism forbidden in the rutile magnetic symmetry ($4'/mm'm$) is allowed in our monoclinic magnetic symmetry (2/m) [22].

Bragg spots $(0,\ 1,\ 0)_t$ or $(0,\ 0,\ 1)_m$ correspond to a reflection vector $c^*_m = (2\pi/a)\ (0,\ 1,\ 0)$ parallel to the crystal b axis (cell length $a \approx 4.497$ Å [15]). At the start of an az-

imuthal angle scan $b_m^* = (2\pi/a)\ (-1,\ 0,\ 0)$ is in the plane of scattering. $E1$–$E1$ amplitudes and the chiral signature are neatly expressed in terms of four purely real quantities,

$$A_1 = \sqrt{2}\left[c\langle T_\zeta^1\rangle + s\langle T_\xi^1\rangle\right],\ B_1 = \sqrt{2}\left[s\langle T_\zeta^1\rangle - c\langle T_\xi^1\rangle\right],$$
$$A_2 = 2\left[c\langle T_{+1}^2\rangle'' - s\langle T_{+2}^2\rangle\right],\ B_2 = 2\left[s\langle T_{+1}^2\rangle'' + c\langle T_{+2}^2\rangle''\right].$$

Note that dipole and quadrupoles here and in neutron diffraction are arranged in different ways. The four amplitudes are (the crystal setting is different from Ref. [23]),

$$\begin{aligned}(\sigma'\sigma) &= A_2 \sin(2\psi),\\ (\pi'\pi) &= i\sin(2\theta)\cos(\psi)\,A_1 + \sin^2(\theta)\sin(2\psi)\,A_2,\\ (\pi'\sigma) &= -i\cos(\theta)\sin(\psi)\,A_1 + i\sin(\theta)\,B_1\\ &\quad + \sin(\theta)\cos(2\psi)\,A_2 - \cos(\theta)\sin(\psi)\,B_2. \end{aligned} \quad (5)$$

A change in sign of A_1 and A_2 relate $(\pi'\sigma)$ and $(\sigma'\pi)$. The Bragg angle for $(0,\ 0,\ 1)_m$ is $\sin(\theta) \approx 0.485$ at the L_3 edge. A chiral signature Υ requires all four amplitudes (Eq. (S2) in the Supplemental Material [7]),

$$\begin{aligned}\Upsilon(c_m^*) &= \cos(\theta)\cos(\psi)\,[\sin(2\theta)\ \sin(\psi)\,(A_1B_2 - B_1A_2)\\ &\quad - 2A_1A_2\{\cos^2(\theta)\sin^2(\psi) + \sin^2(\theta)\}]\cdot(0,\ 0,\ 1)_m\end{aligned} \quad (6)$$

As already mentioned, interference between dipoles (A_1, B_1) and time-even quadrupoles (A_2, B_2) creates Υ. By definition, the chiral signature expresses different phases between the four amplitudes, i.e., it vanishes if all four are purely real or purely imaginary.

The chiral signature for a reflection vector b_m^* parallel to the crystal a axis, with Miller indices $(1,\ 0,\ 0)_t$ or $(0,\ -1,\ 0)_m$, is significantly different from Eq. (6) [23]. A key factor making the difference is that one $(0,\ -1,\ 0)_m$ scattering amplitude is zero. The result in question $(\sigma'\sigma) = 0$ for a reflection vector b_m^* is a specific test of the proposed magnetic symmetry.

IV. CONCLUSIONS

In summary, we studied a magnetic symmetry for RuO_2 that accommodates a Néel vector that is not parallel to the rutile c axis, demanded by magnetic rutile symmetry $(P4_2'/mnm')$. In consequence, it fulfils a theory of anomalous thermal transport coefficients [6]. Magnetic symmetry $P2_1/c$ chosen for study permits a chiral signature in the diffraction of circularly polarized x-rays. We do not find a corresponding chiral signature in magnetic symmetry $Pn'n'm$ used by Šmejkal *et al.* to promote their spontaneous crystal Hall effect in RuO_2 [25]. (Figs. 1D and 2B in Ref. [25] are consistent with magnetic symmetry $Pnn'm'$ and not $Pn'n'm$ mentioned in the text. The chiral signature of $Pnn'm'$ is reported by Lovesey *et al.* [23], where it is labeled motif No. 2.) Notably, $Pn'n'm$ does not descend from the parent rutile structure, and c-axis ferromagnetism and perfectly antiparallel moments in the (ab) plane are permitted. Furthermore, there is no experimental evidence of an orthorhombically distorted structure (cell edges a ≠ b) of RuO_2 consistent with magnetic symmetry Pn′n′m, with Ru ions in sites 2a and ferromagnetic order along the c axis. Another acid test of $P2_1/c$ is the prediction of null Bragg intensity $(1,\ 0,\ 0)_t$ or $(0,\ -1,\ 0)_m$ for unrotated photon polarization. Neutron diffraction amplitudes Eqs. (2), (3), and (4) await tests, as do the x-ray chiral signature Eq. (6) and diffraction amplitudes Eq. (5).

A calculation of the x-ray Bragg diffraction pattern of RuO_2 reported by Zhu *et al.* [26] yields a null chiral signature, because the calculation does not include the 90° phase shift between charge and magnetic contributions to x-ray scattering demanded by magnetic crystal symmetry. According to Zhu *et al.* [26], charge and magnetic contributions to x-ray scattering amplitudes possess a common phase and add in calculations of corresponding intensities, whereas, the contributions are in quadrature in intensities, because charge and magnetic contributions to correct amplitudes are 90° phase shifted with respect to each other.

Regarding neutron diffraction, a zero magnetic quadrupole and zero orbital angular momentum are consistent with a viable interpretation of published data [15]. Specifically, null coupling constants between a state with total angular momentum $J = 0$ in the Ru^{4+} ground state and $J' = 1, 2$, i.e., $\chi(J')_r = 0$, noting that the multipole rank = J′. A zero magnetic quadrupole is alien to altermagnetism, because the result implies a strong spin-orbit coupling, the likes of which is found in iridates, for example [3,24]. The incomplete theory is probably justified in some cases, but it is definitely not a general concept, and in each case, one needs to decide to what extent the approach is applicable. Our exact neutron form factors for the atomic configuration d^4 and symmetry exact diffraction amplitudes enable a peerless confirmation of $P2_1/c$ magnetic symmetry of RuO_2, or its emphatic rejection.

[1] I. Turek, Phys. Rev. B **106**, 094432 (2022).

[2] L. Šmejkal, J. Sinova, and T. Jungwirth, Phys. Rev. X **12**, 040501 (2022).

[3] D. D. Khalyavin and S. W. Lovesey, Phys. Rev. B **100**, 224415 (2019).

[4] F. E. Neumann, *Vorlesungen über die Theorie Elasticität der festen Körper und des Lichtäthers* (Teubner, Leipzig, 1885).

[5] A. P. Cracknell, *Magnetism in Crystalline Materials* (Pergamon Press, Oxford, 1975).

[6] X. Zhou, W. Feng, R.-W. Zhang, L. Smejkal, J. Sinova, Y. Mokrousov, and Y. Yao, arXiv:2305.01410.

[7] See Supplemental Material at http://link.aps.org/supplemental/10.1103/PhysRevB.108.L121103 for detailed structure information and x-ray scattering process, which includes Ref. [8].

[8] We use the BNS setting of magnetic space groups, see Bilbao Crystallographic server, http://www.cryst.ehu.es.

[9] J. Hubbard and W. Marshall, Proc. Phys. Soc. **86**, 561 (1965); I. Sovago, M. J. Gutmann, J. G. Hill, H. M. Senn, L. H. Thomas, C. C. Wilson, and L. J. Farrugia, Cryst. Growth Des. **14**, 1227 (2014).

[10] S. W. Lovesey, *Theory of Neutron Scattering from Condensed Matter*, Vol. 2 (Clarendon Press, Oxford, 1987).

[11] R. D. Cowan, J. Opt. Soc. Am. **58**, 808 (1968).
[12] S. W. Lovesey, D. D. Khalyavin, and G. van der Laan, Phys. Rev. B **99**, 134444 (2019).
[13] S. W. Lovesey, Phys. Scr. **90**, 108011 (2015).
[14] A. T. Boothroyd, *Principles of Neutron Scattering from Condensed Matter* (OUP, Oxford UK, 2020).
[15] T. Berlijn, P. C. Snijders, O. Delaire, H.-D. Zhou, T. A. Maier, H.-B. Cao, S.-X. Chi, M. Matsuda, Y. Wang, M. R. Koehler, P. R. C. Kent, and H. H. Weitering, Phys. Rev. Lett. **118**, 077201 (2017).
[16] J. Fernández-Rodríguez, S. W. Lovesey, and J. A. Blanco, Phys. Rev. B **77**, 094441 (2008).
[17] V. Scagnoli and S. W. Lovesey, Phys. Rev. B **79**, 035111 (2009).
[18] J. Luo, G. T. Trammell, and J. P. Hannon, Phys. Rev. Lett. **71**, 287 (1993).
[19] C. Vettier, J. Electron Spectrosc. Relat. Phenom. **117–118**, 113 (2001).
[20] L. Paolasini, De La Société Française De La Neutronique (SFN) **13**, 03002 (2014).
[21] S. W. Lovesey, E. Balcar, K. S. Knight, and J. Fernández-Rodríguez, Phys. Rep. **411**, 233 (2005).
[22] B. T. Thole, P. Carra, F. Sette, and G. van der Laan, Phys. Rev. Lett. **68**, 1943 (1992); P. Carra, B. T. Thole, M. Altarelli, and X. D. Wang, *ibid.* **70**, 694 (1993); P. Carra, H. König, B. T. Thole, and M. Altarelli, Physica B **192**, 182 (1993).
[23] S. W. Lovesey, D. D. Khalyavin, and G. van der Laan, Phys. Rev. B **105**, 014403 (2022).
[24] I. Mazin and the PRX Editors, Phys. Rev. X **12**, 040002 (2022).
[25] L. Šmejkal, R. González-Hernández, T. Jungwirth, and J. Sinova, Sci. Adv. **6**, eaaz8809 (2020).
[26] Z. H. Zhu, J. Strempfer, R. R. Rao, C. A. Occhialini, J. Pelliciari, Y. Choi, T. Kawaguchi, H. You, J. F. Mitchell, Y. Shao-Horn, and R. Comin, Phys. Rev. Lett. **122**, 017202 (2019).